nature physics

Article

https://doi.org/10.1038/s41567-023-02206-0

Electronic origin of high superconducting critical temperature in trilayer cuprates

In the format provided by the authors and unedited

Supplementary Section 1. The maximized T_c in Bi2223 and its persistence in the overdoped region

Supplementary Section 2. Characterization of the Bi2223 single crystal samples for the ARPES measurements

Supplementary Section 3. Band splitting along the nodal direction between the α and β bands

Supplementary Section 4. Photoemission spectra (EDCs) of Bi2223 measured along the three Fermi surface sheets at 18K

Supplementary Section 5. Global simulations of the observed three Fermi surface, band structures, superconducting gap and the selective Bogoliubov band hybridizations in the superconducting state of overdoped Bi2223

Supplementary Section 6. Simulated band structures of Bi2223 by considering the interlayer hopping t_{io} only

Supplementary Section 7. Simulated band structures of Bi2223 by considering the individual effect of interlayer hopping, superconducting gap and interlayer pairing

Supplementary Section 8. The effect of the interlayer pairing Δ_{oo} on the gap structure of Bi2223

Supplementary Section 9. Fitting of the hybridization between the β Bogoliubov band and the γ band in the superconducting state of overdoped Bi2223

1. The maximized T_c in Bi2223 and its persistence in the overdoped region

Figure S1a shows the maximum T_c as a function of the number of CuO_2 planes in the Bi-, Tl- and Hg-based homologous series of cuprates[1–4]. It was found that within the same series the maximum T_c is realized for n=3.

Figure S1b shows the doping dependence of T_c in Bi2212 and Bi2223[5, 6]. Bi2212 shows a normal phase diagram where T_c is a maximum at the optimal doping; it decreases with increasing doping in the overdoped region. On the other hand, Bi2223 exhibits an unusual phase diagram. In the overdoped region, its T_c keeps nearly constant with increasing doping.

2. Characterization of the Bi2223 single crystal samples for the ARPES measurements

The Bi2223 single crystals used in our ARPES measurements were post-annealed under high oxygen pressure. They are overdoped. We carried out AC magnetic measurements on the samples and the measured result is shown in Fig. S2. It shows a T_c at 108.0 K and a sharp superconducting transition with a width of 3.0 K.

3. Band splitting along the nodal direction between the α and β bands

Figure S3b shows the original data measured along the nodal direction at 18 K in Bi2223. The corresponding MDC at the Fermi level is shown in Fig. S3a. Fig. S3d shows the MDC second derivative image of the original band in Fig. S3b. The corresponding second derivative MDC at the Fermi level from Fig. S3d is shown in Fig. S3c. In the measurement, not only the three main bands (α, β and γ) are observed, but also their corresponding superstructure bands are observed on the right side of the images in Fig. S3(b,d). There is a band splitting between the α and β bands, as seen clearly from their superstructure bands in Fig. S3b and more clearly seen in the second derivative image in Fig. S3d. In fact, the strong main peak in the MDC (Fig. S3a) and the second derivative MDC (Fig. S3c) consists of a main peak and a shoulder. By fitting the two main peaks with three Lorentzians and the one superstructure peak with two Lorentzians in Fig. S3a, we can get a consistent band splitting of $0.011\pi/a$ between the α and β bands and the band splitting of $0.075\pi/a$ between the α and γ bands. These results indicate that the trilayer splitting, particularly the splitting between the α and β bands, is present even along the nodal direction in overdoped Bi2223.

4. Photoemission spectra (EDCs) of Bi2223 measured along the three Fermi surface sheets at 18K

Figure S4 shows the EDCs along the α (Fig. S4a), β (Fig. S4b) and γ (Fig. S4c) Fermi surface of Bi2223. The peak positions of the α, β and γ bands are marked by ticks in Fig. S4a, S4b and S4c, respectively. For the EDCs along the γ Fermi surface (Fig. S4c), the EDC peak splits into two near the antinodal region. This is due to the Bogoliubov band hybridization between the β and γ bands.

5. Global simulations of the observed three Fermi surface, band structures, superconducting gap and the selective Bogoliubov band

hybridizations in the superconducting state of overdoped Bi2223

ARPES measures the single particle spectral function $A(k, \omega)$:

$$I_{ARPES} = I_0 \times A(k, \omega) \times f(\omega, T) \tag{1}$$

where I_0 is a prefactor and $f(\omega, T)$ is the Fermi-Dirac distribution function.

The single particle spectral function $A(k, \omega)$ is the imaginary part of the Green's function $G(k, \omega)$:

$$A(k, \omega) = -\frac{1}{\pi} Im[G(k, \omega)] \tag{2}$$

For describing the superconductivity of the three layer system, we use the full 6×6 matrix Green's function $G(k, \omega)$:

$$G(k, \omega) = (\omega - \Sigma_i(k, w) - H)^{-1} \tag{3}$$

where $\Sigma_i(k, w)$ is the complex self-energy for the band i = IP, OP.

$$\Sigma_i(k, w) = \Sigma_i^{'}(k, w) + i\Sigma_i^{''}(k, w) \tag{4}$$

$\Sigma_i^{'}(k, w)$ and $\Sigma_i^{''}(k, w)$ are the real part and imaginary part of $\Sigma_i(k, w)$, respectively. We simulated the spectrum with self-energy of the marginal Fermi liquid to describe the interaction between the electrons[7, 8].

$$\Sigma_i^{''}(k, w) = \lambda\sqrt{w^2 + (\pi k_B T)^2} + \Gamma_0 \tag{5}$$

The real part is obtained by using the Kramers-Kronig relation:

$$\Sigma^{'}(w) = \frac{1}{\pi} \int \frac{\Sigma^{''}}{\omega^{'} - \omega} d\omega^{'} \tag{6}$$

As described in the main text, the Hamiltonian of the triple-layer cuprate in superconducting state is:

$$H = \Phi^{\dagger} \begin{pmatrix} \epsilon_{op}(k) & t_{io}(k) & t_{oo}(k) & \Delta_{op}(k) & 0 & \Delta_{oo}(k) \\ t_{io}(k) & \epsilon_{ip}(k) & t_{io}(k) & 0 & \Delta_{ip}(k) & 0 \\ t_{oo}(k) & t_{io}(k) & \epsilon_{op}(k) & \Delta_{oo}(k) & 0 & \Delta_{op}(k) \\ \Delta_{op}(k) & 0 & \Delta_{oo}(k) & -\epsilon_{op}(k) & -t_{io}(k) & -t_{oo}(k) \\ 0 & \Delta_{ip}(k) & 0 & -t_{io}(k) & -\epsilon_{ip}(k) & -t_{io}(k) \\ \Delta_{oo}(k) & 0 & \Delta_{op}(k) & -t_{oo}(k) & -t_{io}(k) & -\epsilon_{op}(k) \end{pmatrix} \Phi \tag{7}$$

$$= \Psi^{\dagger} \begin{pmatrix} \epsilon_{op}(k)+t_{oo}(k) & \sqrt{2}t_{io}(k) & 0 & \Delta_{op}(k)+\Delta_{oo}(k) & 0 & 0 \\ \sqrt{2}t_{io}(k) & \epsilon_{ip}(k) & 0 & 0 & \Delta_{ip}(k) & 0 \\ 0 & 0 & \epsilon_{op}(k)-t_{oo}(k) & 0 & 0 & \Delta_{op}(k)-\Delta_{oo}(k) \\ \Delta_{op}(k)+\Delta_{oo}(k) & 0 & 0 & -\epsilon_{op}(k)-t_{oo}(k) & -\sqrt{2}t_{io}(k) & 0 \\ 0 & \Delta_{ip}(k) & 0 & -\sqrt{2}t_{io}(k) & -\epsilon_{ip}(k) & 0 \\ 0 & 0 & \Delta_{op}(k)-\Delta_{oo}(k) & 0 & 0 & -\epsilon_{op}(k)+t_{oo}(k) \end{pmatrix} \Psi \tag{8}$$

Here, $\epsilon_{ip}(k)$ and $\epsilon_{op}(k)$ represent the bare bands of the inner plane and the outer planes, respectively. t_{io} represents the interlayer hopping between the inner and outer planes while t_{oo} represents the interlayer hopping between the two outer planes. Δ_{ip} denotes the intralayer pairing on the inner plane and Δ_{op} denotes the intralayer pairing on the outer planes. Δ_{oo} represents the interlayer pairing between the two outer planes.

The bare band dispersions are given by tight binding model[9]:

$$\epsilon_i(k) = -2t_i[\cos(k_xa)+\cos(k_ya)] - 4t_i^{'}\cos(k_xa)\cos(k_ya) - 2t_i^{''}[\cos(2k_xa)+cos(2k_ya)] - \mu_i, \tag{9}$$

To satisfactorily describe the observed Fermi surface (Fig. 2b), band structures, superconducting gap and Bogoliubov band hybridizations (Fig. 2d), we take (in units of eV) $t_{IP} = 0.123$, $t_{IP}^{'} = -0.37t_{IP}$, $t_{IP}^{''} = -0.47t_{IP}^{'}$ and $\mu_{IP} = -0.092$ for the inner plane (IP) and $t_{OP} = 0.171$, $t_{OP}^{'} = -0.42t_{OP}$, $t_{OP}^{''} = -0.16t_{OP}^{'}$ and $\mu_{OP} = -0.251$ for the outer planes (OP).

It is reasonable to use different intralayer hopping parameters for the inner and outer CuO_2 planes because (1) The inner and outer CuO_2 planes have different environment. The inner plane is sandwiched between two Ca layers in which each Cu is coordinated with four in-plane oxygens. On the other hand, each outer plane is sandwiched between a Ca layer and a SrO layer in which each Cu is coordinated with four in-plane oxygens and one apical oxygen. The different environment and different coordination of Cu may lead to different intralayer hopping parameters; (2) Experimentally, it was shown that the intralayer hopping parameters change with the doping level[10]. Since the doping levels of the inner plane (p∼0.08) and the outer planes (p∼0.30) are very different, they may lead to different intralayer hopping parameters. This is why different intralayer hopping parameters were used to fit the band structures of Bi2223 in the previous ARPES studies by Ideta et al.[11–13] and Kunisada et al.[14]. We tried to fit our data by using the same intralayer hopping parameters for the inner plane and outer planes. It is possible to fit the three observed Fermi surface sheets well. But when we simulated the band structure in the superconducting state by using these parameters, the simulated results deviate strongly from the measured ones. This indicates that it is not possible to get a global fitting of the Fermi surface, band structures, superconducting gaps and selective Bogoliubov band hybridization if the intralayer hopping parameters of the inner and outer CuO_2 planes are taken the same.

Usually, the interlayer hopping t_{io} is assumed to increase monotonically from the nodal to the antinodal regions[13, 14]: $t_{io}(k) = t_{io0} + t_{io1}[\cos(k_x a) - \cos(k_y a)]^2/4$. Fig. S5 shows such a t_{io} with t_{io0}=0 and t_{io1}=103 meV (red triangles). As described in the main text, such t_{io} is not consistent with the experimental result (Fig. 4d). To match the measured results, we take the form $t_{io}(k) = \cos(k_x a/2)\cos(k_y a/2)(t_{io0} + t_{io1}[\cos(k_x a) - \cos(k_y a)]^2/4)$. which is shown in Fig. S5 as black circles with t_{io0}=0 and t_{io1}=103 meV. It is strong in the middle region and is suppressed near the antinodal region. In the simulation (Fig. 2f), we take a strongly anisotropic $t_{oo}(k) = t_{oo0} + t_{oo1}[\cos(k_x a) - \cos(k_y a)]^2/4$ where t_{oo0}=-6 meV and t_{oo1}=-53.3 meV (red line in Fig. 2f). The intralayer pairing potential in plane i is: $\Delta_i(k) = \Delta_i^0[\cos(k_x a) - \cos(k_y a)]/2$ where we take Δ_{op}^0=20 meV and Δ_{ip}^0=65 meV. The interlayer pairing Δ_{oo} also takes the same d-wave form with Δ_{oo}^0=5 meV (Fig. 2g).

6. Simulated band structures of Bi2223 by considering the interlayer hopping t_{io} only

Figure S6a shows the simulated band structures of Bi2223 along different momentum cuts from nodal to antinodal regions. Here in the simulation, we considered the interlayer hopping t_{io} only without considering t_{oo}. The measured band structures are shown in Fig. S6b for direct comparison. In this case, it is still possible to make the simulated Fermi surface match the measured ones. But the parameters in the tight binding model of the bare bands need to be adjusted. In particular, a momentum dependent t_{io} has to take a form of $t_{io} = t_{io0} + t_{io1}[cos(k_x a) - cos(k_y a)]^2/4$ with t_{io0}=21.9 meV and t_{io1}=94.8 meV. The simulated band structures (Fig. S6a) show significant discrepancies from the measured results (Fig. S6b). The most notable difference is that in the simulated band structures (Fig. S6a), the Bogoliubov band hybridization always occurs between the α and γ bands while in the measured results (Fig. S6b), the hybridization is actually between the β and γ bands. In addition, in the simulated band structures (Fig. S6a), the Bogoliubov band hybridization increases dramatically and monotonically from the nodal to the antinodal regions. But in the measured band structures (Fig. S6b), the band hybridization is strong in the intermediate range between the nodal and the antinodal regions and becomes rather weak near the antinodal region. These results indicate that it is impossible to describe the measured results by considering only the interlayer hopping between the inner and outer CuO_2 planes (t_{io}) and t_{oo} is significant and must be included in the simulation.

One may wonder whether it is possible to understand the experimental results by considering t_{oo} only without t_{io}. The answer is no because t_{oo} does not produce Bogoliubov band hybridization, as seen from the diagonalized Hamiltonian (Eq. 8) and simulated results in Fig. S7(g,o). The clear observation of the Bogoliubov band hybridization indicates that t_{io} plays an indispensable role in Bi2223.

7. Simulated band structures of Bi2223 by considering the individual effect of interlayer hopping, superconducting gap and interlayer pairing

In order to disentangle the effect of each term in Eq. 1 in the main text, we carried out the band structure simulations by gradually adding more terms onto the bare band case, as shown in Fig. S7. From left to right panels, we simulated the band structures by considering bare bands (left panels), adding t_{io} only (second left panels), adding t_{oo} only (second right panels) and adding both t_{io} and t_{oo} (right panels). From top to bottom panels, we simulated the band structures by considering bare bands (top panels), adding Δ_{ip} and Δ_{op} (second top panels), adding Δ_{ip}, Δ_{op} and Δ_{io} (second bottom panels) and adding Δ_{ip}, Δ_{op} and Δ_{oo} (bottom panels). Fig. S7(a-d) shows the simulated band structures in the normal state while Fig. S7(e-p) shows the band structures in the superconducting state.

8. The effect of the interlayer pairing Δ_{oo} on the gap structure of Bi2223

Figure S8 shows the measured and simulated band structures of Bi2223 along the momentum cut with θ=18^o close to the antinodal region. All the parameters used in the simulation are the same as those used in Fig. 2 except for Δ_{oo}. Fig. S8b shows the simulated band structure without Δ_{oo} while Fig. S8c shows the simulated band structure with Δ_{oo}=3.8 meV. Without Δ_{oo}, the superconducting gaps of the α and β bands show a small difference (Fig. S8b) that is not consistent with the measured result (Fig. S8a). Only after considering Δ_{oo}, the superconducting gaps of the α and β bands (Fig. S8c) become consistent with the measured result (Fig. S8a).

9. Fitting of the hybridization between the β Bogoliubov band and the γ band in the superconducting state of overdoped Bi2223

As seen in the above Eq. 8, the band hybridization occurs only between the β and γ bands. In order to quantitatively fit the band hybridization, we rewrite a 4×4 Hamiltonian:

$$H_{\beta\gamma} = \Psi^\dagger \begin{pmatrix} \epsilon_{op}(k) + t_{oo}(k) & \sqrt{2}t_{io}(k) & \Delta_{op}(k) + \Delta_{oo}(k) & 0 \\ \sqrt{2}t_{io}(k) & \epsilon_{ip}(k) & 0 & \Delta_{ip}(k) \\ \Delta_{op}(k) + \Delta_{oo}(k) & 0 & -\epsilon_{op}(k) - t_{oo}(k) & -\sqrt{2}t_{io}(k) \\ 0 & \Delta_{ip}(k) & -\sqrt{2}t_{io}(k) & -\epsilon_{ip}(k) \end{pmatrix} \Psi \tag{10}$$

$$= \Phi^\dagger \begin{pmatrix} \epsilon_\beta(k) & t_\perp(k) & \Delta_\beta(k) & 0 \\ t_\perp(k) & \epsilon_\gamma(k) & 0 & \Delta_\gamma(k) \\ \Delta_\beta(k) & 0 & -\epsilon_\beta(k) & -t_\perp(k) \\ 0 & \Delta_\gamma(k) & -t_\perp(k) & -\epsilon_\gamma(k) \end{pmatrix} \Phi \tag{11}$$

In this case, $\epsilon_\beta(k) = \epsilon_{op}(k)+t_{oo}(k)$, $\epsilon_\gamma(k) = \epsilon_{ip}(k)$, $t_\perp(k) = \sqrt{2}t_{io}(k)$, $\Delta_\beta(k) = \Delta_{op}(k) + \Delta_{oo}(k)$ and $\Delta_\gamma(k) = \Delta_{ip}(k)$.

The eigenvalues of the hybridized bands are then given by[13]:

$$E^2 = \frac{E_\beta^2 + E_\gamma^2}{2} + t_\perp^2(k) \pm \sqrt{(\frac{E_\beta^2 - E_\gamma^2}{2})^2 + t_\perp^2(k)[(\epsilon_\beta(k) + \epsilon_\gamma(k))^2 + (\Delta_\beta(k) - \Delta_\gamma(k))^2]}. \tag{12}$$

where $E_\beta^2 = \epsilon_\beta^2(k) + \Delta_\beta^2(k)$ and $E_\gamma^2 = \epsilon_\gamma^2(k) + \Delta_\gamma^2(k)$.

Figure S9a shows the band structures of Bi2223 measured along ten momentum cuts from the nodal to the antinodal regions at 18 K in the superconducting state. Fig. S9b shows the fitted band structures of β and γ bands. Since the fitted energy range is relatively small (<80 meV), we took parabolic form for the $\epsilon_\beta(k)$ and $\epsilon_\gamma(k)$ bare bands. The fitted band structures of the hybridized β and γ bands in Fig. S9b are in a good agreement with the measured bands in Fig. S9a. In particular, we show the data and their fittings near the antinodal region with θ=15-20 in Fig. S10. As seen from the original data (Fig. S10a), the second derivative images (Fig. S10b) and the EDCs at the hybridization momentum k_h (Fig. S10c), the band structures around the momentum-energy region of the band hybridization between the β Bogoliubov back-bending band and the γ band exhibit a systematic and monotonic variation with the momentum cuts from θ=20 to θ=15. The Bogoliubov band hybridization for the momentum Cut1 (θ=20) is strong and obvious (topmost panels in Fig. S10(a,b)) which can be well fitted by simulations (topmost panel in Fig. S10c). The Bogoliubov band hybridization for the momentum Cut6 (θ=15) is nearly invisible (bottom panels in Fig. S10(a,b)) which can also be well fitted by simulations (bottom panel in Fig. S10c). Therefore, it is reasonable that the hybridization gap gradually decreases from a finite value for θ=20 to nearly zero for θ=15 although the relative uncertainty of the extracted hybridization gap gets larger because of the weak overall signal and the decreasing Bogoliubov band hybridization. The extracted t_{io} is shown in Fig. 4d and the extracted $\Delta_\beta(k)$ and $\Delta_\gamma(k)$ are shown in Fig. 4h, named as $\Delta_{F\beta}(k)$ and $\Delta_{F\gamma}(k)$, respectively.

---

[1] H. Mukuda, S. Shimizu, A. Iyo and Y. Kitaoka. High-Tc superconductivity and antiferromagnetism in multilayered copper oxides -a new paradigm of superconducting mechanism. *Journal of the Physical Society of Japan* **81**, 011008 (2012).

[2] C. W. Chu, L. Z. Deng and B. Lv. Hole-doped cuprate high temperature superconductors. *Physica C* **514**, 290 (2015).

[3] I. Bozovic, J. N. Eckstein and G. F. Virshup. Superconducting oxide multilayers and superlatlices: physics, chemistry, and nanoengineering. *Physica C* **235**, 178 (1994).

[4] H. Wang, X. L. Wang, S. X. Shang, Z. Wang, Z. K. Lu and M. H. Jiang. Possible presence of 2234 phase with T_c(zero) of 95 K in a Bi-Pb-Sb-Sr-Ca-Cu-O ceramic. *Applied Physics Letters* **57**, 710 (1990).

[5] T. Fujii, I. Terasaki, T. Watanabe, and A. Matsuda. Doping dependence of anisotropic resistivities in the trilayered superconductor $Bi_2Sr_2Ca_2Cu_3O_{10+\delta}$. *Physical Review B* **66**, 024507 (2002).

[6] A. Piriou, Y. Fasano, E. Giannini, and ϕ. Fischer. Effect of oxygen-doping on

$Bi_2Sr_2Ca_2Cu_3O_{10+\delta}$ vortex matter: crossover from electromagnetic to Josephson interlayer coupling. *Physical Review B* **77**, 184508 (2008).

[7] C. M. Varma, P. B. Littlewood, S. Schmitt-Rink, E. Abrahams and A. E. Ruckenstein. Phenomenology of the normal state of Cu-O high-temperature superconductors. *Physical Review Letters* **63**, 1996 (1989).

[8] H. X. Li, X. Q. Zhou, S. Parham, T. J. Reber, H. Berger, G. B. Arnold, and D. S. Dessau. Coherent organization of electronic correlations as a mechanism to enhance and stabilize high-Tc cuprate superconductivity. *Nature Communications* **9**, 26 (2018).

[9] R. S. Markiewicz, S. Sahrakorpi, M. Lindroos, H. Lin and A. Bansil. One-band tight-binding model parametrization of the high-T_c cuprates including the effect of k_z dispersion. *Physical Review B* **72**, 054519 (2005).

[10] Y. G. Zhong, Y. M. Chen, J. Y. Guan, J. Zhao, Z. C. Rao, C. Y. Tang, H. J. Liu, Y. J. Sun and H. Ding. Extraction of tight binding parameters from in-situ ARPES on the continuously doped surface of cuprates. *Science China-Physics, Mechanics and Astronomy.* **61**, 127403 (2018).

[11] S. Ideta, K. Takashima, M. Hashimoto, T. Yoshida, A. Fujimori, H. Anzai, T. Fujita, Y. Nakashima, A. Ino, M. Arita, H. Namatame, M. Taniguchi, K. Ono, M. Kubota, D. H. Lu, Z.-X. Shen, K. M. Kojima, and S. Uchida. Enhanced superconducting gaps in the trilayer high-temperature $Bi_2Sr_2Ca_2Cu_3O_{10+\delta}$ cuprate superconductor. *Physical Review Letters* **104**, 227001 (2010).

[12] S. Ideta, K. Takashima, M. Hashimoto, T. Yoshida, A. Fujimori, H. Anzai, T. Fujita, Y. Nakashima, A. Ino, M. Arita, H. Namatame, M. Taniguchi, K. Ono, M. Kubota, D. H. Lu, Z.-X. Shen, K. M. Kojima and S. Uchida. Angle-resolved photoemission study of the tri-layer high-Tc superconductor $Bi_2Sr_2Ca_2Cu_3O_{10+\delta}$: effects of inter-layer hopping. *Physica C* **470**, S14 (2010).

[13] S. Ideta, S. Johnston, T. Yoshida, K. Tanaka, M. Mori, H. Anzai, A. Ino, M. Arita, H. Namatame, M. Taniguchi, S. Ishida, K. Takashima, K. M. Kojima, T. P. Devereaux, S. Uchida, and A. Fujimori. Hybridization of Bogoliubov quasiparticles between adjacent CuO_2 layers in the triple-layer cuprate $Bi_2Sr_2Ca_2Cu_3O_{10+\delta}$ studied by angle-resolved photoemission spectroscopy. *Physical Review Letters* **127**, 217004 (2021).

[14] S. Kunisada, S. Adachi, S. Sakai, N. Sasaki, M. Nakayama, S. Akebi, K. Kuroda, T. Sasagawa,

T. Watanabe, S. Shin, and T. Kondo. Observation of Bogoliubov band hybridization in the optimally doped trilayer $Bi_2Sr_2Ca_2Cu_3O_{10+\delta}$. *Physical Review Letters* **119**, 217001 (2017).

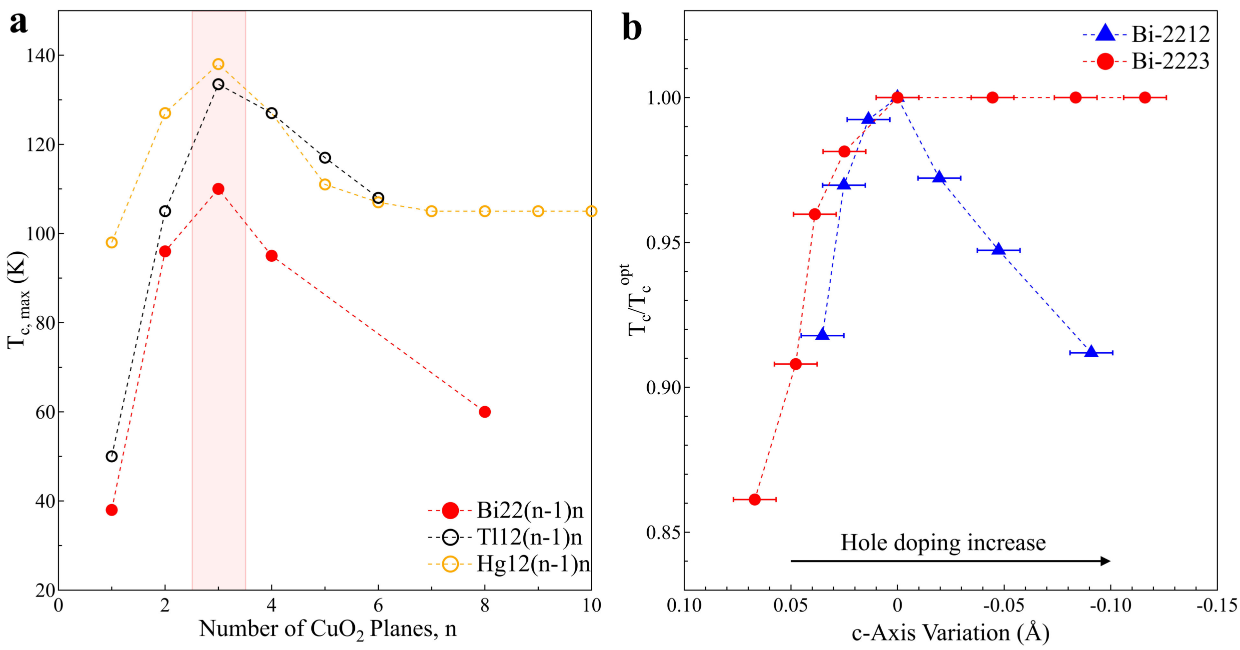

FIG. S1. T_c **dependence on the number of** CuO_2 **planes (n) and on the doping levels in high temperature cuprate superconductors.** (a) Relationship between the maximum T_c ($T_{c,max}$) and n for the homologous series of cuprates in different systems[1–4]. (b) Unique doping dependence of T_c in Bi2223[5, 6]. Normalized T_c as a function of the variation of the c-axis lattice constant in the annealed Bi2212 and Bi2223 samples which is reproduced from[5]. The uncertainties are ± 0.01 $\AA$ as marked by error bars. Here, the decrease of the c-axis lattice constant corresponds to the increase of the hole doping level. In Bi2212, T_c exhibits a maximum at the optimal doping and then decreases with increasing doping in the overdoped region. In Bi2223, T_c exhibits a maximum at the optimal doping and then keeps nearly constant with increasing doping in the overdoped region.

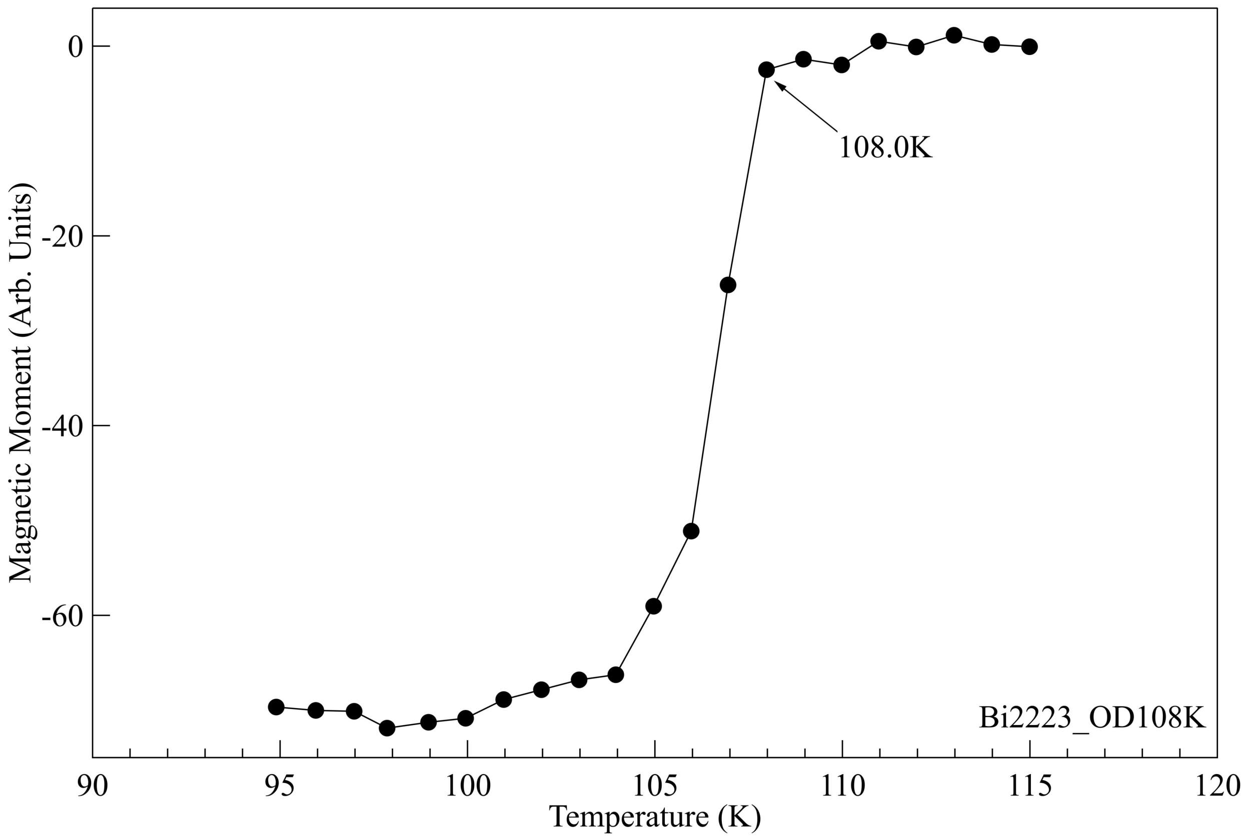

FIG. S2. **Magnetic AC susceptibility of the Bi2223 single crystal measured by the present ARPES experiments.** The measured superconducting transition temperature (T_c) is 108.0 K with a transition width of ∼3.0 K. The sample is overdoped after it was annealed under high oxygen pressure of ∼170 atmospheres.

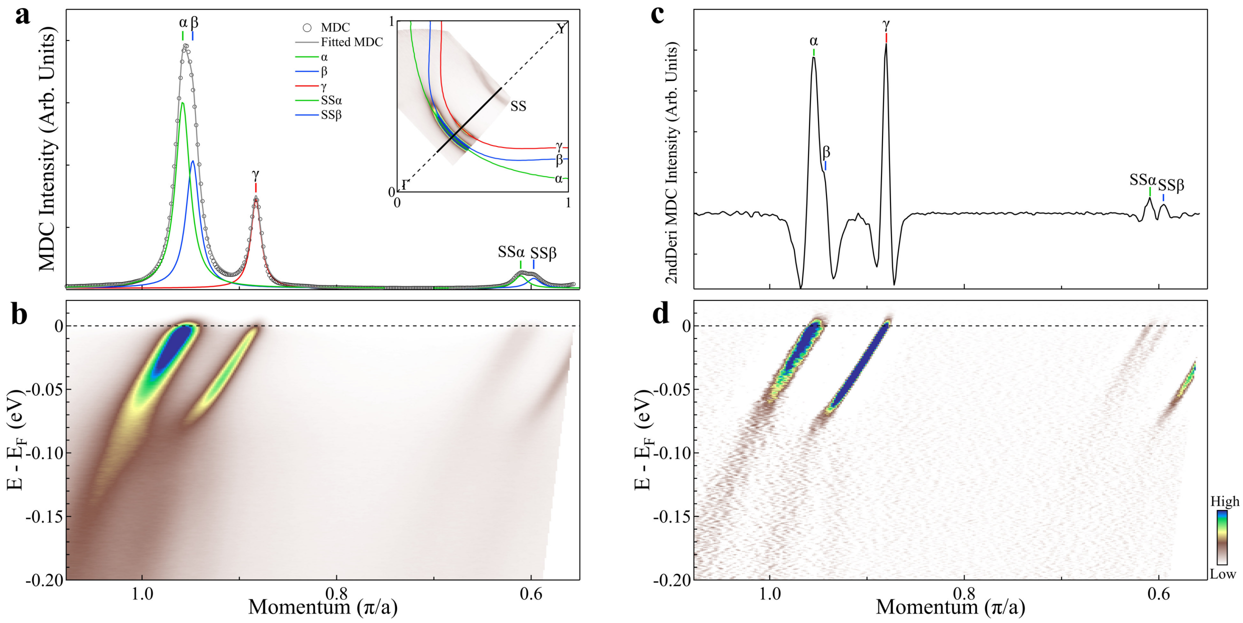

FIG. S3. **Observation of trilayer splitting in the measured band structure of Bi2223 along the nodal direction.** (a-b) Band structure measured at 18 K along the nodal direction (b) and the corresponding MDC at the Fermi level (a). The location of the nodal momentum cut is marked by the black line in the inset of (a). Both the main bands (α, β and γ) and the superstructure bands ($SS\alpha$ and $SS\beta$) are observed and marked. (c-d) The corresponding MDC second derivative image (d) obtained from (b) and the second derivative MDC at the Fermi level (c). In addition to the band splitting between the (α, β) and γ bands, the band splitting between the α and β bands is also clearly observed which is more obvious in the superstructure bands and particularly clear in the second derivative image (d) and second derivative MDC (c). The main band MDC (black empty circles) in (a) is fitted by taking three Lorentzians that represent three main bands of α (green line), β (blue line) and γ (red line). The superstructure band MDC (black empty circles) in (a) is fitted by taking two Lorentzians that represent two superstructure bands of $SS\alpha$ (green line) and $SS\beta$ (blue line). The extracted band splitting between the α and γ bands is $0.075\,\pi/a$ while the splitting between the α and β bands is $0.011\,\pi/a$.

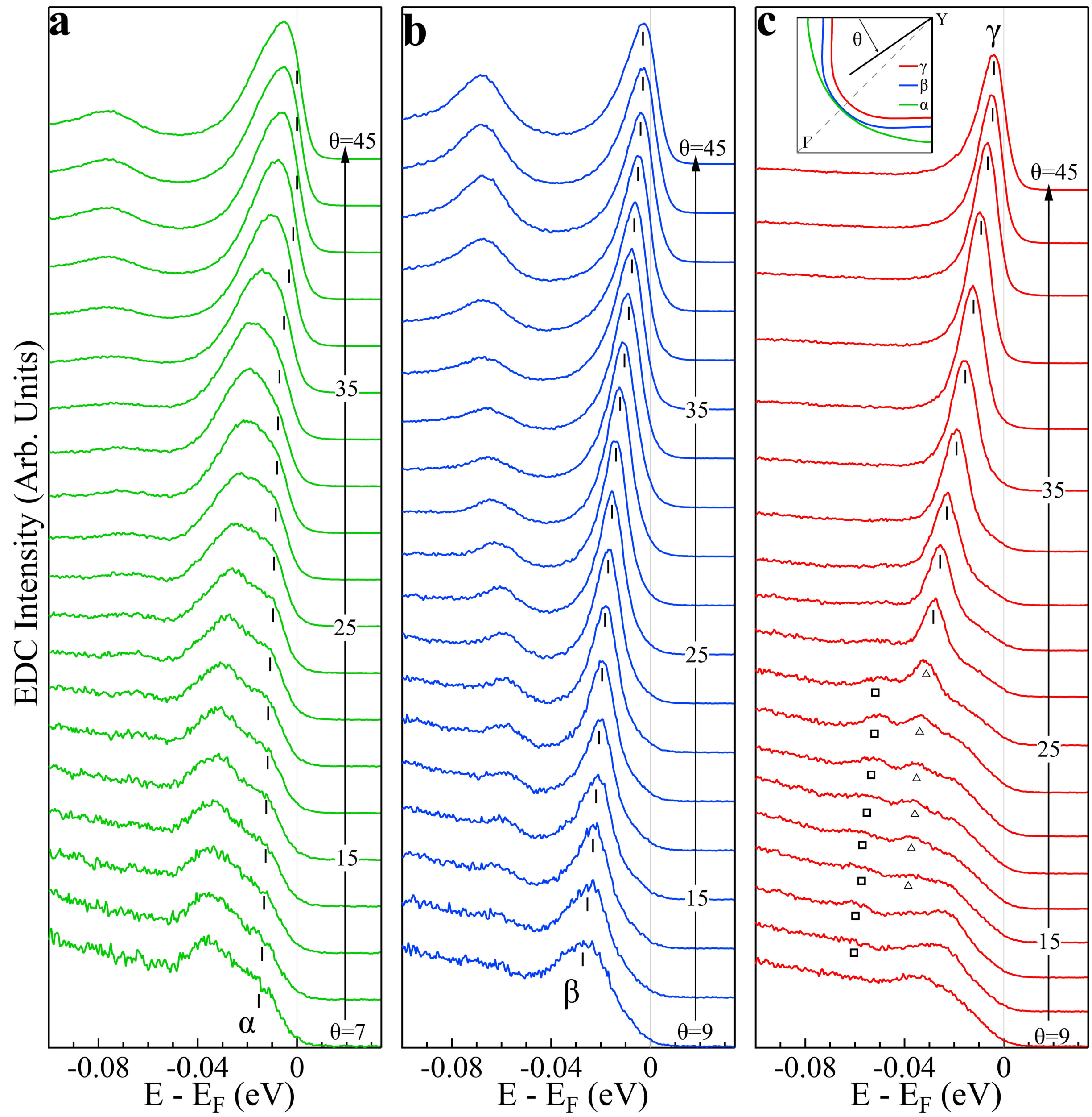

FIG. S4. **Photoemission spectra (energy distribution curves, EDCs) of Bi2223 along the three Fermi surface sheets measured at 18 K.** (a-c) shows EDCs along the α (a), β (b) and γ (c) Fermi surface sheets, respectively. The location of the Fermi momentum is defined by the angle θ, as shown in the inset of (c) where $\theta = 0$ corresponds to the $(0, \pi)$ antinodal region while $\theta = 45$ corresponds to the nodal region. The EDC peaks that correspond to α band are marked by ticks in (a); they are on the shoulders of the EDC peaks of the underlying β band. The EDC peaks that correspond to β band are marked by ticks in (b). For the EDCs along the γ Fermi surface, one main peak is observed near the nodal region with $\theta = 45 \sim 27$ as marked by ticks in (c). Towards the antinodal region with $\theta = 25 \sim 15$, two EDC peaks are observed due to band hybridization, as marked by triangles and squares in (c).

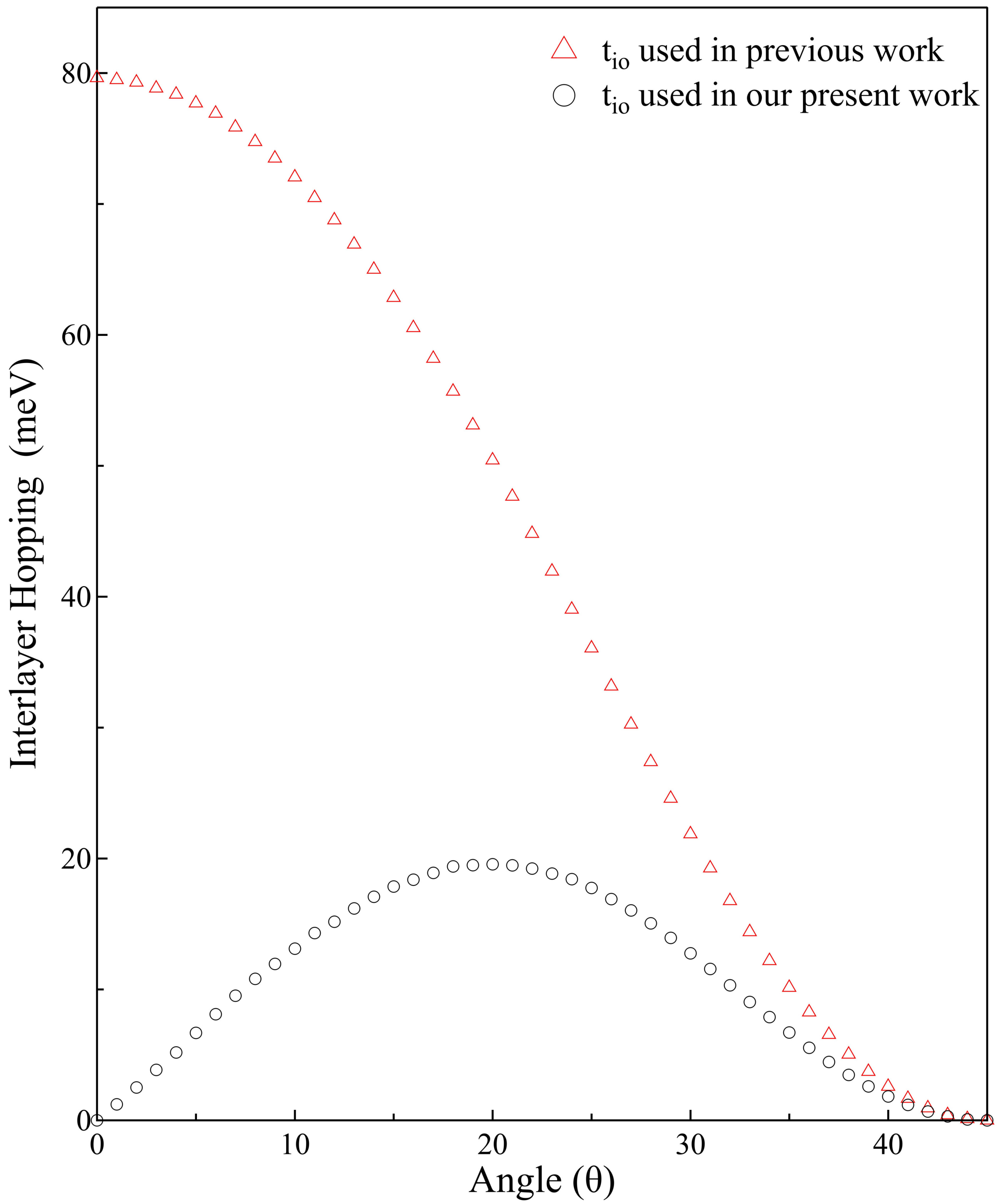

FIG. S5. **The interlayer hopping t_{io} used in the simulation.** The form of t_{io} used in the previous work[13, 14] and in our present work are plotted by red triangles and black circles, respectively. The location of the Fermi momentum is defined by the angle θ, the same as that defined in the inset of Fig. S4c, where $\theta = 0$ corresponds to the $(0, \pi)$ antinodal region while $\theta = 45$ corresponds to the nodal region.

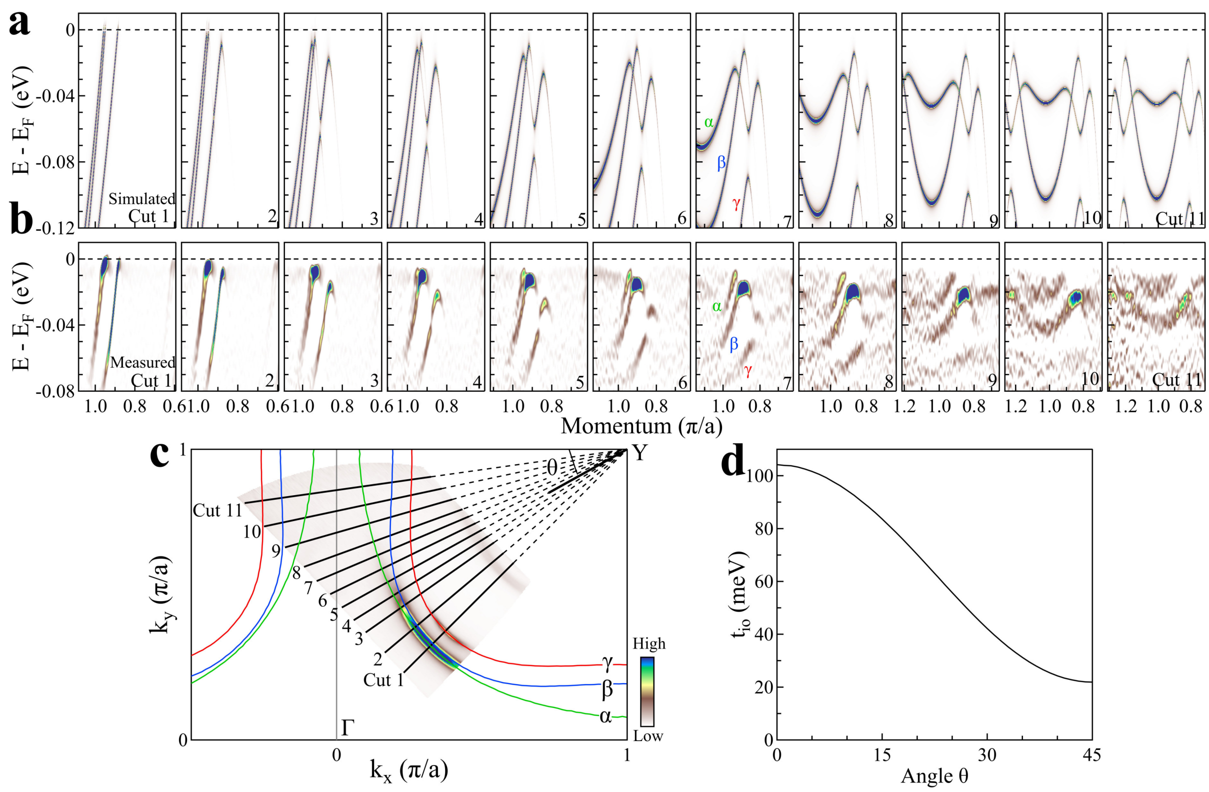

FIG. S6. **Simulated band structures of Bi2223 by considering the interlayer hopping t_{io} only.** (a) Simulated band structures along different momentum cuts from nodal to antinodal regions. The location of momentum cuts is shown in (c) by black lines. (b) The measured band structures of Bi2223 along the same eleven momentum cuts. These are the EDC second-derivative images. (c) The simulated Fermi surface sheets, α (green line), β (blue line) and γ (red line), that are in good agreement with the measured Fermi surface. The location of momentum cuts are marked and the Fermi surface angle θ is defined. (d) Momentum dependent t_{io} used in the simulation. It has a form of $t_{io} = t_{io0} + t_{io1}[cos(k_x a) - cos(k_y a)]^2/4$ with t_{io0}=21.9 meV and t_{io1}=94.8 meV.

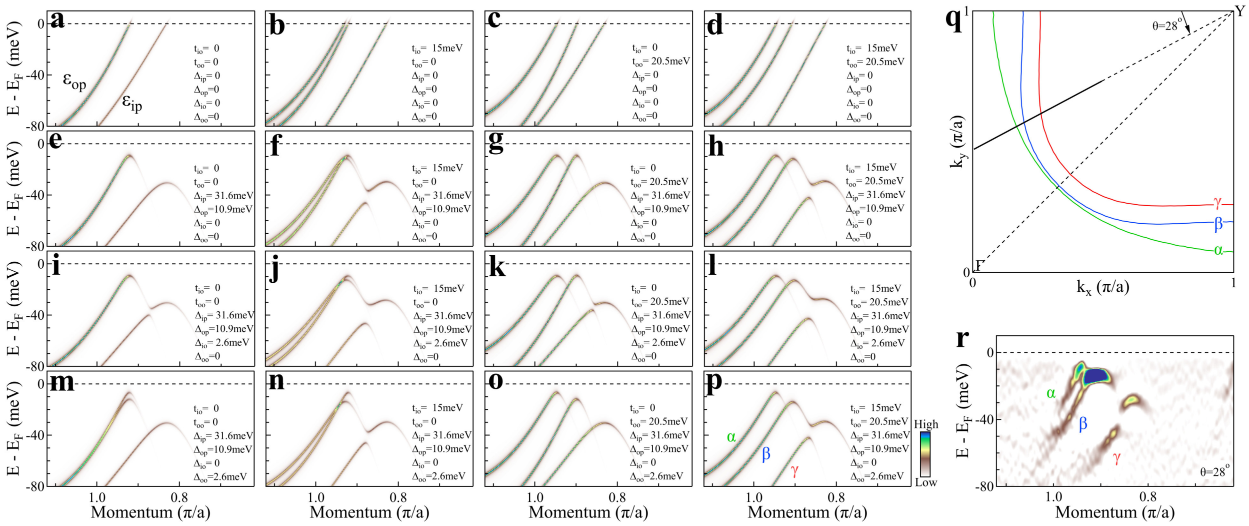

FIG. S7. **Simulated band structures along a momentum cut in the normal and superconducting states of Bi2223 by considering the individual effect of interlayer hopping, superconducting gap and interlayer pairing.** (a) shows the bare bands of the inner plane (IP) and outer plane (OP) while (b-d) show three bands that are produced after the introduction of the interlayer couplings: t_{io} only, t_{oo} only and both t_{io} and t_{oo}, respectively, in the normal state. The location of the momentum cut is shown in (q) as a black line. (e-h) show the band structures in the superconducting state obtained from (a-d) after the superconducting gaps Δ_{ip} and Δ_{op} are introduced to the inner plane and outer plane, respectively. (i-l) show the band structures in the superconducting state obtained from (e-h) when the interlayer pairing between the inner and outer planes, Δ_{io}, is added. (m-p) show the band structures in the superconducting state obtained from (e-h) when the interlayer pairing between the outer planes, Δ_{oo}, is added. (q) Fermi surface of Bi2223 and the location of the momentum cut. (r) A typical band structure measured along the same momentum cut with $\theta = 28°$. It is the EDC second-derivative image.

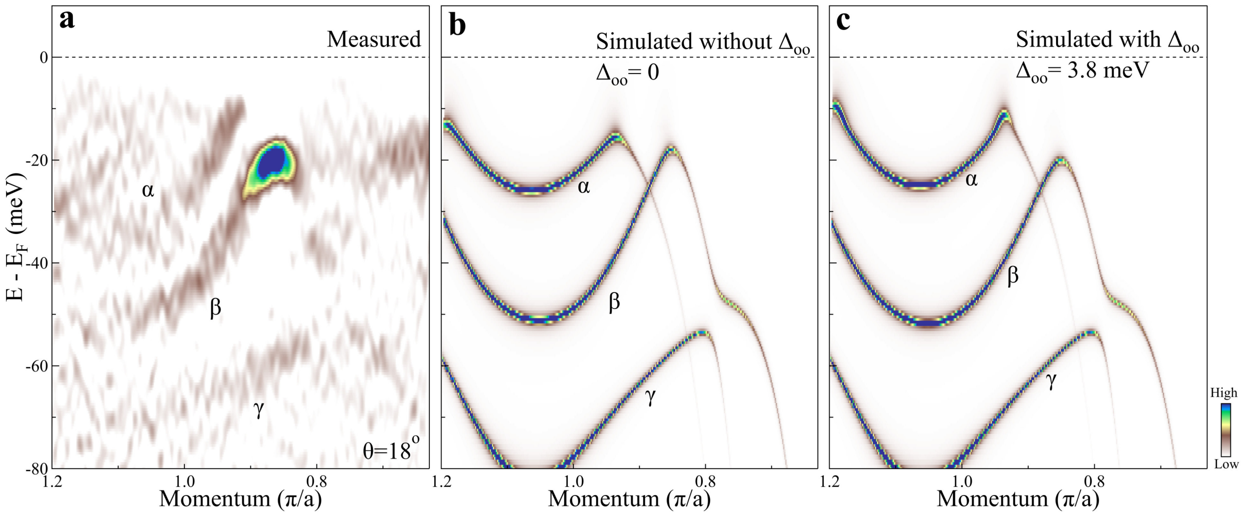

FIG. S8. **The effect of the interlayer pairing Δ_{oo} on the gap structure of Bi2223.** (a) A typical band structure measured along the momentum cut with $\theta = 18°$. It is the EDC second-derivative image. The α and β bands show different gap size. (b) Simulated band structure along the same momentum cut without considering Δ_{oo}. In this case, the gap size between the α and β bands is small which is not consistent with the measured result in (a). (c) Simulated band structure along the same momentum cut by considering Δ_{oo}. In this case, the gap size between the α and β bands becomes obviously different which becomes consistent with the measured result in (a).

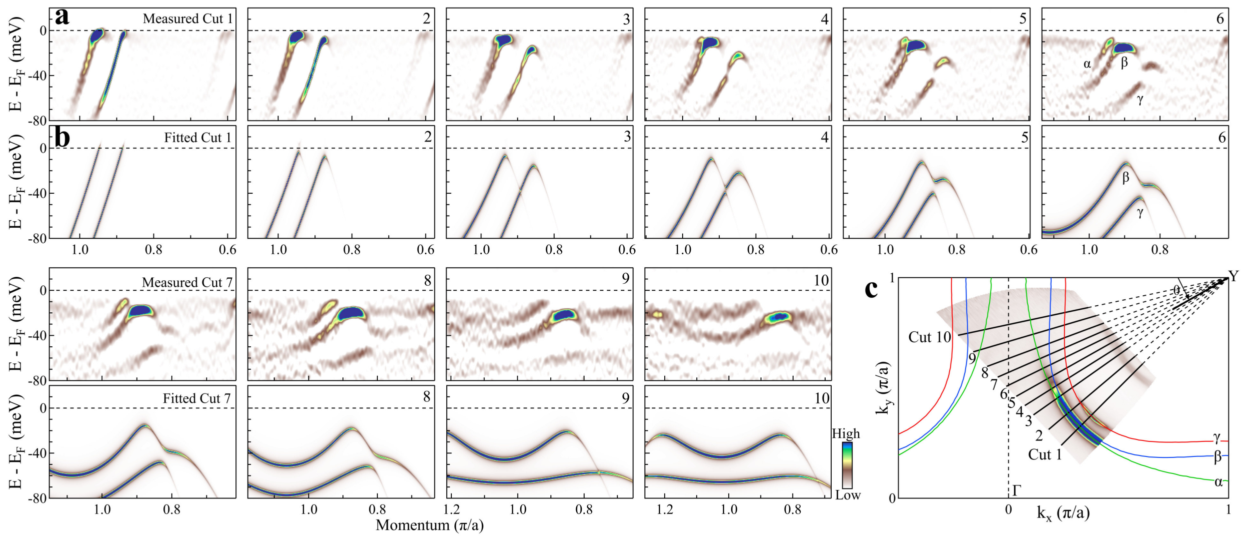

FIG. S9. **Fitting of the band hybridization between the β Bogoliubov band and the γ band in Bi2223.** (a) Band structures measured along ten typical momentum cuts. The location of the momentum cuts is marked by black lines in (c). These are EDC second derivative images which can show the band hybridization between the β and γ bands more clearly. (b) Fitted band structures along the same ten momentum cuts as in (a) by considering the band hybridization of the β and γ bands. (c) Fermi surface of Bi2223 and the location of the momentum cuts.

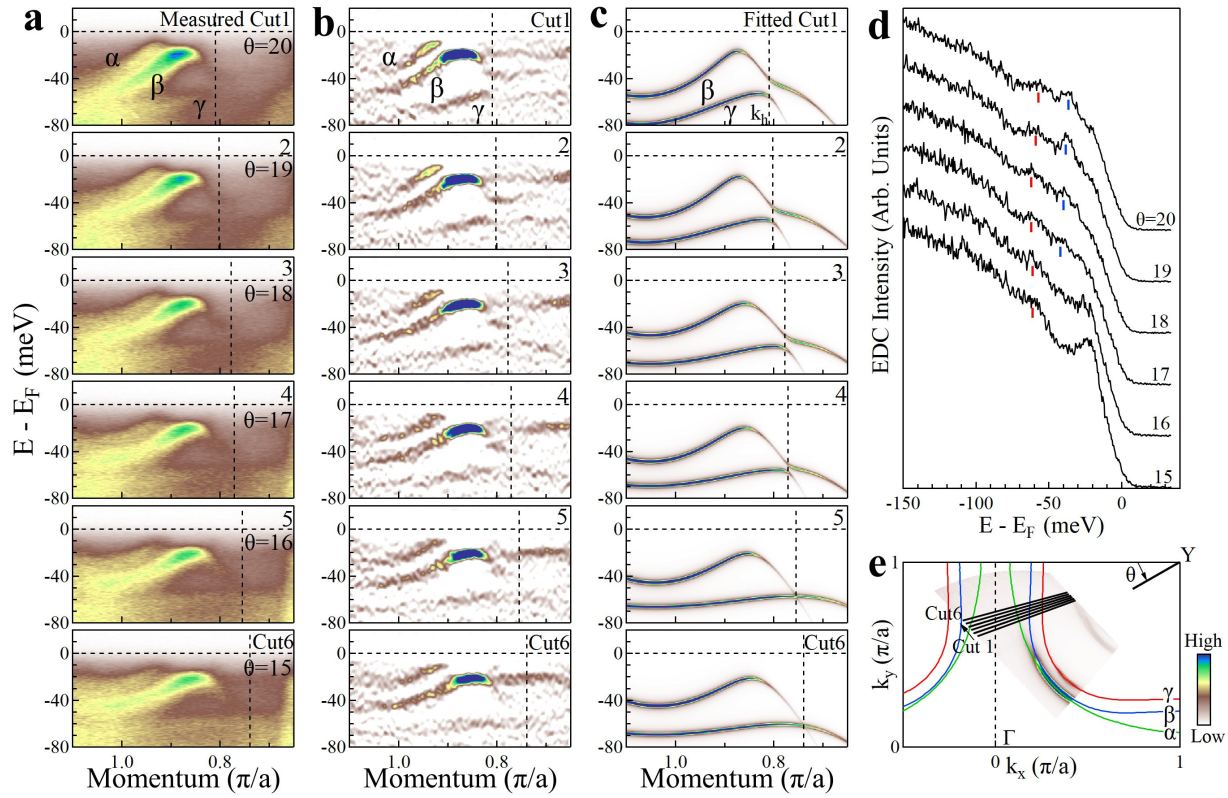

FIG. S10. **Momentum dependent evolution of the band hybridization between the β Bogoliubov band and the γ band in Bi2223 near the antinodal region.** (a) Band structures measured along six momentum cuts. The location of the momentum cuts is marked by black lines in (e). (b) Corresponding EDC second derivative images obtained from (a). (c) Fitted band structures along the same six momentum cuts as in (a) and (b) by considering the band hybridization of the β and γ bands. (d) EDCs at the hybridization momentum obtained from (a). The position of the hybridization momentum (k_h) is marked by the vertical dashed line in (a,b,c). The hybridization gap forms at k_h due to the Bogoliubov band hybridization, giving rise to two branches of bands at the hybridization momentum. The features in EDCs corresponding to the lower branch are marked by red ticks while those corresponding to the upper branch are marked by blue ticks. (e) Fermi surface of Bi2223 and the location of the momentum cuts.